

A simple method for improving crustal corrections in waveform tomography

V. Lekić,¹ M. Panning² and B. Romanowicz¹

¹Berkeley Seismological Laboratory, 225 McCone Hall, University of California, Berkeley, CA 94720, USA. E-mail: lekic@seismo.berkeley.edu

²Department of Geological Sciences, 241 Williamson Hall, University of Florida, Gainesville, FL 32611, USA

Accepted 2010 March 15. Received 2010 February 19; in original form 2009 July 9

SUMMARY

Accurate accounting for the effects of crustal structure on long-period seismic surface waves and overtones is difficult but indispensable for determining elastic structure in the mantle. While standard linear crustal corrections (SLC) have been shown to be inadequate on the global scale, newer non-linear correction (NLC) techniques are computationally expensive when applied to waveforms containing higher frequencies and/or overtones. We devise, implement, and verify a modified SLC approach that mimics the non-linear effects of the crust without substantially increasing the computational costs. While theoretically less accurate than the NLC approach, in practice, the reduced computational costs allow this ‘modified linear correction’ (MLC) technique to be applied at higher frequencies and using more detailed crustal regionalizations than is possible with NLC. In order to validate the MLC technique, we use the spectral element method to carry out a series of synthetic tests. These tests demonstrate that MLC nearly eliminates the contamination of mantle isotropic structure by unmodelled crustal effects, which can be substantial in the uppermost 150 km when using SLC. Furthermore, we show that MLC significantly reduces contamination of anisotropic structure compared to SLC, the inaccuracies of which are significant in the upper 250 km and can even obliterate the mantle anisotropic signature at depths shallower than 100 km. Finally, we apply the MLC technique to a real long period waveform data set and demonstrate the benefit of improved crustal corrections on the retrieved model.

Key words: Surface waves and free oscillations; Seismic tomography; Computational seismology; Crustal structure.

1 INTRODUCTION

Recordings of surface waves and overtones provide unparalleled constraints on the structure of the Earth’s crust (e.g. Meier *et al.* 2007), upper mantle (e.g. Montagner & Tanimoto 1991), and transition zone (e.g. Ritsema *et al.* 2004). This is because they offer excellent global coverage, and are sensitive to elastic and anelastic structure in both the crust and the mantle. Yet, in order to determine the seismic velocities and anisotropy in the mantle, we must disentangle the effects of the crust from those due to the sought-after mantle structure. The ability of crustal effects to significantly affect retrieved models of mantle velocities, even at long periods and on large scales, was recognized as early as the pioneering work of Woodhouse & Dziewonski (1984). Accounting for the effects of crustal structure requires knowing the velocity structure of the crust as well as accurately calculating the effects of that structure on surface waves and overtones.

A number of efforts at determining the elastic structure of the crust have been carried out over the past decade. Global tomographers have typically relied on models of crustal structure derived from other data sets, such as refraction and reflection seis-

mics, receiver functions and geological data, (e.g. 3SMAC: Nataf & Ricard 1996; CRUST5.1: Mooney *et al.* 1998; CRUST2.0: Bassin & Masters 2000), in order to predict and correct for crustal effects. More recently, global and regional crustal thickness and velocity models derived solely from surface wave data have been developed (e.g. Pasyanos 2005; Meier *et al.* 2007).

Yet, since accurately modelling the effects of the crust on waves can be difficult, improved maps of crustal structure do not automatically translate into improved corrections for crustal effects. Within a normal mode formalism, which is useful for constructing and analysing long-period waveforms, the effects of heterogeneity on waveforms can be expressed as shifts to the Earth’s eigenfrequencies, as well as the displacement field (eigenfunction) associated with each vibrational mode. Woodhouse & Dziewonski (1984) applied linear corrections, in which eigenfrequency shifts due to crustal structure are calculated in a 1-D model, but the perturbations to the eigenfunctions are neglected, in order to remove the effect of the ocean–continent crustal dichotomy from long period waveforms. Due to their minimal computational costs, linear corrections have found widespread use (e.g. Gu *et al.* 2003; Chevrot & Zhao 2007). Li & Romanowicz (1996) went one step beyond

simply performing linear crustal corrections, and allowed perturbations to the Mohorovičić (Moho) depth in the inversion, which partially accounted for unmodelled crustal effects.

However, variations in crustal thickness are often too large to be accurately handled by linear corrections. In particular, the large differences in Moho depth between platforms, shields, orogens, continental margins, and ocean basins, change the shape of the eigenfunctions, thereby affecting the eigenfrequencies in a significantly non-linear fashion (Montagner & Jobert 1988). Boschi & Ekström (2002) accounted for these non-linear effects by calculating perturbations to the phase of fundamental-mode surface waves exactly at each point along the source–receiver ray path. However, calculating the effects of crustal structure on complete seismic waveforms requires accounting for coupling between normal modes, which is computationally expensive even when dealing with a single set of eigenfunctions. If applied to complete seismic waveforms, Boschi’s approach would require calculating coupling among modes in dozens (if not hundreds) of sets of eigenfunctions, and is unfeasible. A workaround to this problem was proposed by Montagner & Jobert (1988), who suggested a two-step approach in which the eigenfunctions and eigenfrequencies are calculated exactly for a set of representative tectonic settings (instead of for the exact earth structure beneath every point along the ray path); perturbations away from these canonical 1-D profiles are handled using linear corrections. Recently, this approach was independently implemented in full-waveform analyses by Kustowski *et al.* (2007) and Marone & Romanowicz (2007). Two global shear wave speed and radial anisotropic models (Panning & Romanowicz 2006; Kustowski *et al.* 2008) have been developed using these non-linear crustal corrections (henceforth referred to as NLC).

It is important to note that these approaches, while capturing some of the non-linearity associated with wave propagation through a heterogeneous crust, fail to explicitly take into account 3-D finite-frequency effects calculated for the relevant 3-D crustal model. Furthermore, the NLC approach treats deviations from a small set of reference regions in a linear fashion; because increasing the number (N_r) of these reference regions results in substantial computational cost increases, the method is applicable only when the non-linear effects are not too strong. Finally, even when the linear corrections away from these reference regions are sufficiently accurate, NLC requires N_r times more calculations and memory than SLC. Since the number of modes increases as the square of maximum frequency, the significant computational costs of NLC make it ill-suited for use at high frequencies.

These drawbacks of NLC motivated us to develop an alternative method for performing crustal corrections, which could approximate the non-linear effects, but without substantially increasing computational costs. Like the aforementioned methods, we calculate exactly the eigenfunctions and eigenfrequencies for a set of tectonic settings, but instead of using these directly, we solve for scaling coefficients, which, when applied to standard linear crustal corrections, mimic the non-linear effects. We call this approach ‘modified linear corrections’ (MLC). It is based on empirically modifying the topography of crustal discontinuities so that the predictions of linear theory better approximate the crustal corrections obtained by accounting for non-linear effects. In the MLC approach, only a single set of eigenfunctions is required for performing crustal corrections, albeit at a cost of introducing some inaccuracy compared to NLC. This inaccuracy is, to an extent, offset by the fact that a larger number of reference regions can be implemented. Thus, the main advantage of the MLC approach is that, once the correction factors have been calculated, it requires no additional computational costs

aside from those associated with linear corrections. This allows it to be applied to higher frequencies and at much finer regionalizations than possible with NLC.

We then proceed to validate our approach using a synthetic data set generated using the Coupled Spectral Element Method (Capdeville *et al.* 2003). First, we quantify the contamination of mantle models developed using full-waveform inversion that can result from the use of SLC; then, we demonstrate that our MLC method effectively suppresses this contamination. Our approach for quantifying mantle contamination arising from crustal corrections is similar to that of Bozdağ & Trampert (2008) who undertook a thorough analysis of crustal effects on phase velocities of surface waves. Unlike that study, however, we model the complete seismic waveform in order to not discard amplitude information. Also, our use of finite-frequency kernels in the vertical plane allows us to investigate crustal effects on overtones, which were not analysed by Bozdağ & Trampert (2008).

2 THEORETICAL BACKGROUND

In this study, waveform modelling is accomplished within a normal mode formalism, which lends itself to constructing and analysing long period waveforms. Within this formalism, an acceleration time-series is represented as a summation of the contributions of a set of discrete, orthonormal modes of oscillation, each vibrating at a frequency ω_k ,

$$u(t) = \sum_k A_k \exp(i\omega_k t). \quad (1)$$

The modes’ displacement field is represented radially by a set of functions identified by index n , and laterally by spherical harmonics of degree l and order m . For convenience, we will use the index k to identify a mode defined by indices (n, l, m) . The eigenfrequencies and eigenfunctions for a given 1-D earth model can be calculated using computationally efficient codes such as MINEOS (Woodhouse 1998). The $2l + 1$ modes with the same l and n are collectively referred to as a multiplet, and in a spherically symmetric model, they all have the same frequency. Source excitation and receiver orientation are represented by A_k , and the expressions for its constituent parts can be found in Woodhouse & Girnius (1982).

First order perturbation theory can be used to account for effects of non-spherically symmetric structure (e.g. Woodhouse & Dahlen 1978). In this approach, 3-D structure perturbs the frequencies of modes within a multiplet (called splitting), and couples energy within and between multiplets of similar frequency. Calculating the coupling between all possible pairs of modes can be computationally very expensive, so additional approximations have been used in order to make the problem computationally tractable.

Romanowicz (1987) showed that considering coupling along a single mode branch (all l and m for a given n) is, for large l , equivalent to accounting for average radial structure (1-D) along the great circle path from source to receiver. This coupling can be represented by introducing a correction factor $\delta\tilde{\omega}_k$ to ω_k in eq. (1), which quantity can be obtained by integrating along the great circle joining source and receiver the local frequency shifts $\delta\omega_k$ resulting from coupling within an individual multiple induced by 3-D structure,

$$\delta\tilde{\omega}_k = \frac{1}{\Delta} \int_0^\Delta \delta\omega_k(s) ds, \quad (2)$$

where Δ is the epicentral distance.

This approach, first implemented by Woodhouse & Dziewonski (1984), is appropriately called the path average approximation

(henceforth, PAVA). Expressing the frequency shifts in the exponential has the benefit of somewhat relaxing the short-time limitation of standard first order perturbation theory by accounting for multiple forward scattering.

For the case relevant to this study, in which only the radii of discontinuities r_d in the Earth are perturbed by δr_d , local frequency shifts due to coupling within a multiplet can be calculated in a linear fashion through the use of sensitivity kernels H_k^d , the expressions for which can be found on pages 350–351 of Woodhouse & Dahlen (1978). Note that these kernels are calculated for the spherically symmetric reference model. Thus, the frequency shifts resulting from discontinuity topography (e.g. the Moho or the surface, or discontinuities within the crust) are given by,

$$\delta\omega_k^2 \equiv 2\omega_k\delta\omega_k = \sum_d r_d^2 \delta r_d H_k^d. \quad (3)$$

While the path average approximation is highly successful at modelling fundamental mode surface waves, it fails to capture the depth dependent sensitivity of overtone branches (Li & Romanowicz 1995). That is why, when calculating the effects of Earth structure on overtones, we must consider coupling between multiplets k and k' across branches (different n 's) (Li & Tanimoto 1993). Doing this accounts for finite frequency effects of wave sensitivity within the plane defined by the great circle joining source with receiver. In this study, we rely on Non-linear Asymptotic Coupling Theory (NACT; Li & Romanowicz 1995), which is an implementation of across-branch coupling that relies upon asymptotic expressions for spherical harmonics. In it, a linear correction term δu that captures the effects of cross-branch coupling is added to eq. (1)

$$\delta u(t) = \sum_k \left[-it A_k \delta \tilde{\omega}_k + \sum_{k' \subset \Gamma_k} D_{kk'} A_{kk'} \right], \quad (4)$$

with

$$D_{kk'} = \frac{\exp(i\tilde{\omega}_k t) - \exp(i\tilde{\omega}_{k'} t)}{(\omega_k + \omega_{k'}) (\tilde{\omega}_k - \tilde{\omega}_{k'})}, \quad (5)$$

$A_{kk'}$ are the asymptotic forms of scattering integrals, and are given by

$$A_{kk'} = \frac{1}{2\pi} \int_0^{2\pi} \delta\omega_{kk'}^2 \left[Q_{kk'}^{(1)} \cos(j\phi) + Q_{kk'}^{(2)} \sin(j\phi) \right] d\phi, \quad (6)$$

where $j \equiv l - l'$ and the expressions for $Q_{kk'}^{(1)}$ and $Q_{kk'}^{(2)}$ can be found in appendix A of Li & Romanowicz (1995).

Now, the local frequency shifts $\delta\omega_{kk'}^2$ represent the frequency shift of mode k due to discontinuity-topography-induced coupling with multiplet k' ,

$$\delta\omega_{kk'}^2 \equiv 2\omega_{kk'}\delta\omega_{kk'} \equiv (\omega_k + \omega_{k'})\delta\omega_{kk'} = \sum_d r_d^2 \delta r_d H_{kk'}^d \quad (7)$$

and the kernels, $H_{kk'}^d$ still refer to the spherically symmetric reference model, and can be found in appendix C of Li & Romanowicz (1996). For more details, see Romanowicz *et al.* (2008).

3 STANDARD LINEAR AND NON-LINEAR CORRECTIONS

In the previous section, we explained how discontinuity topography can be related via sensitivity kernels H_k^d and $H_{kk'}^d$ to normal mode frequency shifts that arise from coupling within ($\delta\omega_k$) and across

($\delta\omega_{kk'}$) multiplets. Regardless of which coupling terms are considered, the frequency shifts resulting from discontinuity topography can be calculated in either a linear way, or a non-linear one, depending on how the sensitivity kernels H_k^d and $H_{kk'}^d$ are calculated. By linear, we mean that only a single set of eigenfunctions and sensitivity kernels H_k^d and $H_{kk'}^d$ —those of a single reference spherically symmetric model—is used in eqs (3) and (7) to calculate $\delta\omega_k$ and $\delta\omega_{kk'}$. Henceforth, we shall denote frequency shifts calculated in this linear fashion with ‘SL’. Calculating the non-linear effect of the actual structure beneath each point along the ray path between source and receiver would entail using many sets of eigenfunctions (and therefore also many sets of sensitivity kernels H_k^d and $H_{kk'}^d$), one for each point along every source-station path considered. This is not feasible at the present time even for long period (>60 s) waveforms, and a workaround is needed. The approximate solution implemented by Marone & Romanowicz (2007) and Kustowski *et al.* (2007) builds upon the work of Montagner & Jobert (1988) who suggested a two-step approach for calculating $\delta\omega_k$ and $\delta\omega_{kk'}$. First, the eigenfrequencies ($\omega_k^{(i)}$) are calculated for a set of canonical models (indexed by i) that are representative of the variability of crustal structure in the region of study. The difference between these eigenfrequencies and those for the reference spherically symmetric model defines the non-linear frequency shift

$$\delta\omega_k^{NL} = \omega_k^{(i)} - \omega_k^{PREM}, \quad (8)$$

Deviations of structure away from the most similar canonical profile are handled in a linear fashion, using eqs (3) and (7) alongside sensitivity kernels calculated for the relevant canonical radial profile, that is, ${}^{(i)}H_k^d$ and ${}^{(i)}H_{kk'}^d$. The discontinuity radius perturbations δr_d are taken with respect to the most similar canonical model, as well. See Marone & Romanowicz (2007) for a more detailed explanation of this approach. Note that even this two-step non-linear approach for performing crustal corrections (hereafter NLC), requires mode coupling to be calculated between modes in all of the canonical profiles when applied to making NACT synthetics; it is, therefore, much more computationally expensive than SLC.

We now proceed to quantify the accuracy of the SLC and NLC approaches. We begin by subdividing the Earth's surface into seven regions with similar crustal thicknesses and ocean depths. We base this regionalization on Moho depth, since it is the dominant parameter governing the seismic response of the crust at long periods. Starting with CRUST2 (Bassin & Masters 2000), we identify six regions characterized by Moho depth range of 10–25, 25–40, 40–50, 50–60, and >60 km. In order to capture the strong effect of a shallow (<2 km) ocean layer that characterizes the continental shelves, we introduce a seventh region. Fig. 1 maps out the geographical extents of the seven regions. For each region, we calculate an average radial profile of density (ρ) and shear (V_S) and compressional (V_P) wave velocity. The parameters characterizing these profiles are shown in Table 1. Armed with a set of radial models that define seven canonical crustal types, we proceed to calculate the eigenfrequencies $\omega_k^{(i)}$ and eigenfunctions of the fundamental and first five overtone mode branches.

For each canonical crustal model i , we can calculate the kernels ${}^{(i)}H_k^d$ that, through eq. (3), relate perturbations in the radii of discontinuities with the resulting frequency shifts $\delta\omega_k$ of mode k . Note that these kernels only capture the effects of coupling within a multiplet, and though we can also calculate the sensitivity kernels for cross-branch coupling ${}^{(i)}H_{kk'}^d$, these are not easily visualized, and are therefore not shown. Fig. 2 shows how sensitivity of fundamental modes to Moho depth and surface topography varies as a function of mode frequency. Similarly, Fig. 3 shows the average

Crustal Type Regionalization

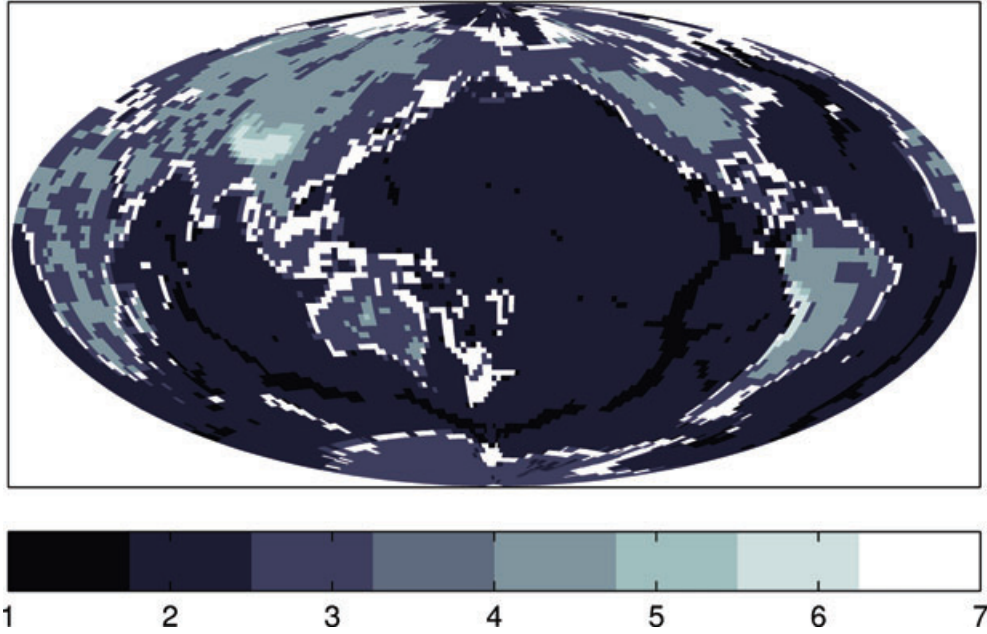


Figure 1. Map showing geographical distribution of the seven crustal types used in this study.

Table 1. Physical parameters characterizing the regions shown in Fig. 1.

Region	Elevation (km)	Moho depth (km)	Density (g cc ⁻¹)	V_p (km s ⁻¹)	V_s (km s ⁻¹)
1	-3.00	9.67	2.86	5.95	3.14
2	-4.22	12.22	2.83	5.66	2.98
3	0.87	34.64	2.82	6.18	3.46
4	0.54	42.60	2.87	6.27	3.52
5	2.82	54.73	2.86	6.35	3.60
6	4.08	64.57	2.88	6.42	3.66
7	-0.80	25.76	2.82	5.71	3.11

Note: Negative elevations are filled with ocean of density 1.02 g cc⁻¹ and V_p 1.45 km s⁻¹.

sensitivities of modes in the first five overtone branches. Note that the basic assumption that underlies standard linear corrections is that discontinuity kernels for different crustal types do not appreciably differ from those of the reference model.

Even a cursory examination of the curves shown in Fig. 2 shows that non-linear effects of surface and Moho topography on fundamental modes dominate at frequencies above 15 mHz. A comparison of the magnitude of the kernels for spheroidal and toroidal modes confirms the well-known fact (Dahlen & Tromp 1998) that toroidal modes are significantly more sensitive to crustal structure than are spheroidal modes. A number of differences between the sensitivity curves indicate that the non-linearity of crustal effects can be non-intuitive. For spheroidal modes, oceanic models with thin crusts are associated with greatest sensitivities to Moho depth. At frequencies higher than 25 mHz, however, a continental-type model takes the lead. For toroidal modes, the story is entirely different, with models with intermediate crustal thicknesses being associated with larger sensitivities to Moho depth than either thin-crust oceanic models or thick crust continental ones. Other examples abound. For instance, note the change in concavity of H_{topo}^S between crustal types 4 and 5, whose crustal thicknesses differ by 12 km. Finally, we point out that for toroidal modes, both surface and Moho kernels are more

similar between models 1 and 6, than they are between 6 and 4, even though differences in crustal structure are far larger between 1 and 6. In short, the condition that discontinuity kernels for different crustal types do not appreciably change is violated even at long periods.

Though the first five overtone branches are significantly less sensitive to topography and Moho depth, Fig. 3 shows that non-linear effects of crustal structure become significant at frequencies higher than ~ 15 mHz. As is the case with the fundamental mode branch, overtones show a number of interesting non-linear effects. For instance, even though toroidal modes are far more sensitive to Moho depth in oceanic models, they are less sensitive to it in PREM than in continental models. This is likely due to the fact that the crust in PREM has two layers, while those of our canonical models have only one. The behavior of spheroidal modes' sensitivities can also be counter-intuitive. First, unlike toroidal modes, spheroidal modes are more sensitive to topography and Moho depth in continental models than in oceanic ones. In fact, spheroidal mode frequencies are several times more sensitive to discontinuity topography in continental, thick-crust models than they are in thin-crust, oceanic models. Interestingly, in models with thick continental crust, the sensitivity of spheroidal modes to discontinuity topography starts to decrease at frequencies above ~ 28 mHz. Thus, even for overtones, non-linear effects of crustal structure cannot be neglected.

We can use discontinuity kernels H_k^d calculated for the reference spherically symmetric model, in this case PREM, to predict the frequency shifts $\delta\omega_k^{(SL)}$ arising from the difference between canonical crustal structures and a spherically symmetric reference model. To do this, we use eq. (3), defining δr_d to be the difference in the radii of the discontinuities between each canonical crustal model and PREM, and neglecting the differences in crustal velocities and density. This is an often used approximation of the true linear crustal effect, and is appropriate because crustal velocities have been shown to have minimal effect on long period waves (e.g. Stutzmann & Montagner 1994). Since the discontinuity

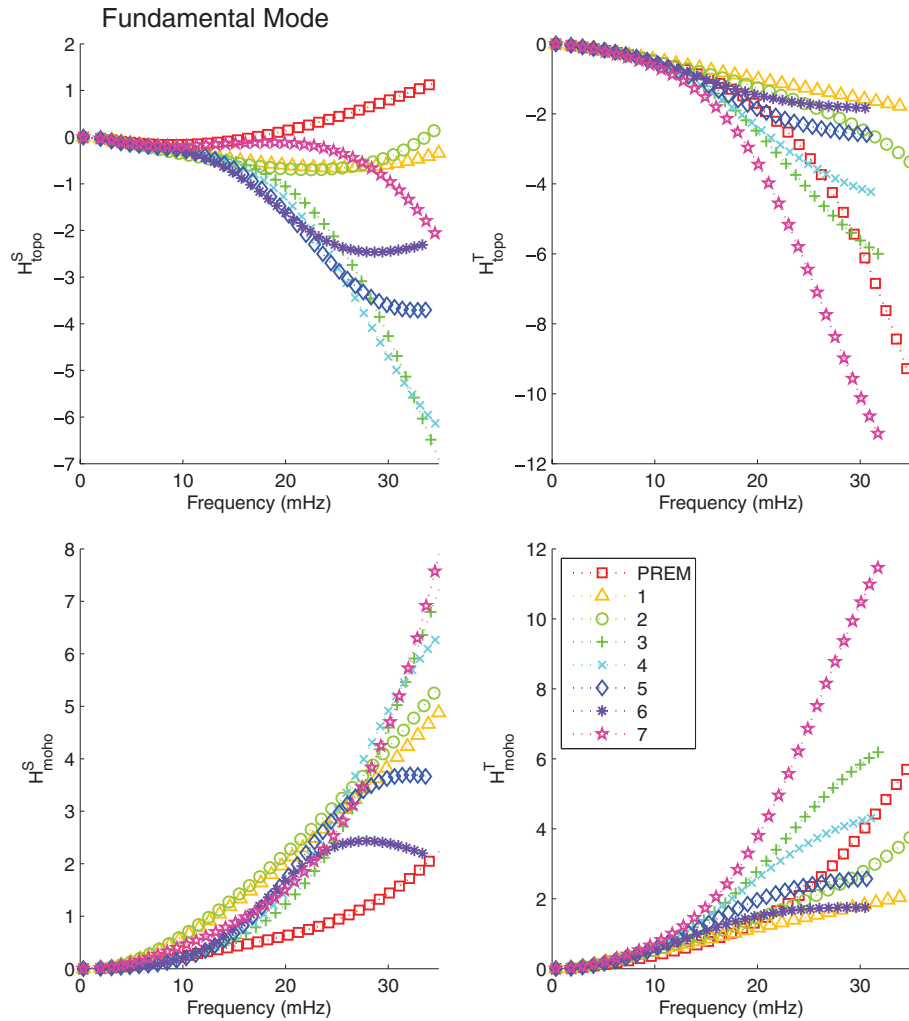


Figure 2. Discontinuity kernels H_k^d for surface topography (top row) and Moho depth (bottom row) as a function of frequency. Spheroidal fundamental modes are in the left-hand column, while toroidal fundamental modes appear on the right-hand column.

perturbations characterizing each canonical model are spherically symmetric (degree zero spherical harmonic), they cannot give rise to coupling of energy between multiplets within a dispersion branch (Dahlen & Tromp 1998, p. 652). As a result, considering coupling within a multiplet is sufficient to accurately model fundamental mode surface waves, and is likely to adequately model overtones as well, since coupling across branches is small, being restricted to only modes with the same l . Therefore, in this test we only consider coupling within a multiplet and use eq. (3) instead of eq. (7) for calculating the frequency shifts. We label the frequency shifts calculated in the standard linear approach $\delta\omega_k^{SL}$. The dotted lines in Figs 4 and 5 show the $\delta\omega_k^{SL}$ for fundamental modes and overtones and each of the canonical crustal structures. A comparison of these approximate terms with the $\delta\omega_k^{NL}$ calculated before (and displayed as solid lines) confirms that linear crustal corrections are inadequate for both fundamental modes and overtones, even at long periods.

4 MODIFIED LINEAR CORRECTIONS

As illustrated in Figs 2–5, SLC corrections are not successful at accounting for the effects of variations in crustal and ocean thickness on surface waves and overtones, even at periods as long

as 100 s. NLC are far more accurate, yet also have substantially greater computation and memory requirements. Therefore, we are interested in ways of correcting the $\delta\omega_k^{SL}$ so that they better track $\delta\omega_k^{NL}$, but also maintain the computational efficiency of SLC. In order to accomplish this task, we are confronted with a crucial choice.

We must decide which term or terms in eq. (3) to refine. Calculating ${}^{(i)}H_k^d$ for each crustal type i , as done in NLC, is a natural choice, since the problem itself is inaccuracy of the linear corrections, rather than the topography of discontinuities. However, since H_k^d needs to be calculated for each mode, and H_{kk}^d for each pair of modes, introducing multiple sets of eigenfunctions is computationally expensive. This is why the computational costs of NLC are so high. Correcting δr_d , on the other hand, does not increase computational costs, since reading one value of δr_d is just as computationally expensive as reading a modified value. The problem with correcting only δr_d , of course, is that it is but a single parameter for a given discontinuity, crustal type, and mode type. Nevertheless, the fact that deviations between $\delta\omega_k^{NL}$ and $\delta\omega_k^{SL}$ change gradually with frequency (see Fig. 4) gives us hope that modifying δr_d might significantly improve the accuracy of $\delta\omega_k^{SL}$.

We start by rewriting eq. (3) to incorporate a topography correction $c_d^{(i)}$ that depends on mode type, discontinuity d , and local

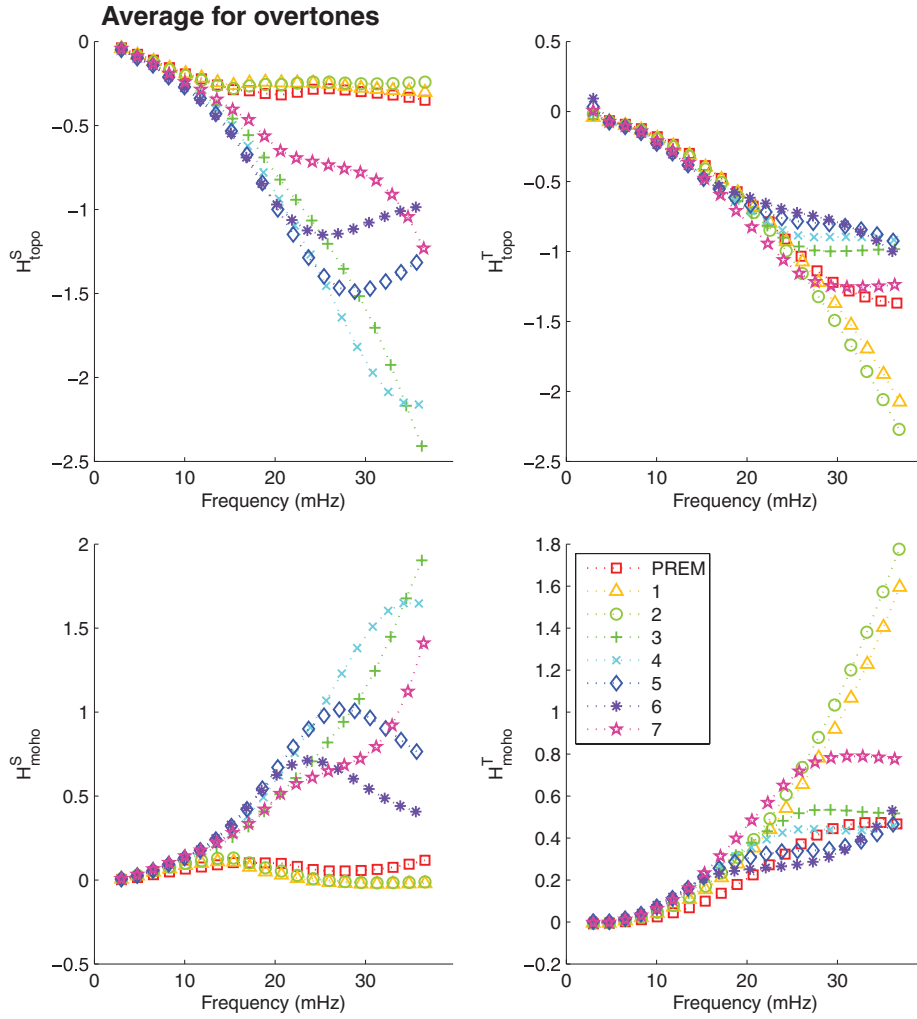


Figure 3. Average discontinuity kernels H_k^d of the first five overtone branches for surface topography (top row) and Moho depth (bottom row) as a function of frequency. Spheroidal modes are in the left-hand column, while toroidal modes appear on the right-hand column.

crustal type i ,

$$\delta\omega_k^{ML} = \frac{1}{2\omega_k} \sum_d r_d^2 (\delta r_d + c_d^{(i)}) H_k^d, \quad (9)$$

or in compact matrix notation as

$$\mathbf{w}^{ML} = \mathbf{H}_0 (\delta \mathbf{r}_0^{(i)} + \mathbf{c}^{(i)}). \quad (10)$$

Note that H_k^d is calculated for the 1-D reference Earth model, and δr_d is with respect to this single reference model. For each canonical crustal type i , we want this modified linear correction ($\delta\omega_k^{ML}$) to be equal to the frequency shift ($\delta\omega_k^{NL}$) calculated in a fully non-linear fashion using eq. (8). The problem, then, reduces to finding the vector of correction terms $\mathbf{c}^{(i)}$ which minimizes the difference between $\delta\omega_k^{ML}$ and $\delta\omega_k^{NL}$; in the least-squares sense, the $\mathbf{c}^{(i)}$ are given by

$$\mathbf{c}_d^{(i)} = (\mathbf{H}_0' \mathbf{H}_0)^{-1} \mathbf{H}_0' (\mathbf{w}_{NL}^{(i)} - \mathbf{H}_0 \delta \mathbf{r}_0^{(i)}), \quad (11)$$

where the apostrophe indicates the transpose.

We could have introduced a multiplicative correction term, instead of the additive one described above. However, solving for such a term becomes unstable when the δr_d 's are small. Given that discontinuity topography is likely to vary both above and below its

depth in the reference model, the accompanying zero-crossings of δr_d will have adverse effects.

Because the non-linearity of crustal effects depends strongly on both crustal and mode type, we perform the minimization in eq. (11) separately for spheroidal and toroidal modes, for fundamental modes and overtones, and for each crustal type. Once the set of factors $\mathbf{c}_{m,t}$ appropriate for a given mode type are obtained, we modify the surface and Moho topography of CRUST2.0 at each point on the surface by the correction factor appropriate for the relevant crustal type (obtained from Fig. 1). Therefore, the crustal type and correction factor information is fused into a single quantity that specifies a modified discontinuity topography for each mode type.

The dashed lines in Figs 4 and 5 show the frequency shifts predicted by our modified discontinuity radii for fundamental modes and overtones, respectively. Henceforth, we label them $\delta\omega_k^{ML}$. For the fundamental modes, the improvement in fit to $\delta\omega_k^{NL}$ is significant over a large frequency range. The fit for the overtones is less good, though still significantly better than that provided by standard linear corrections ($\delta\omega_k^{SL}$). When only long-period waves ($T > 60$ s) are considered, excellent agreement between $\delta\omega_k^{ML}$ and $\delta\omega_k^{NL}$ can even be achieved when only correcting the Moho topography. In the section that follows, we use uncorrected surface topography, modifying only the Moho radii.

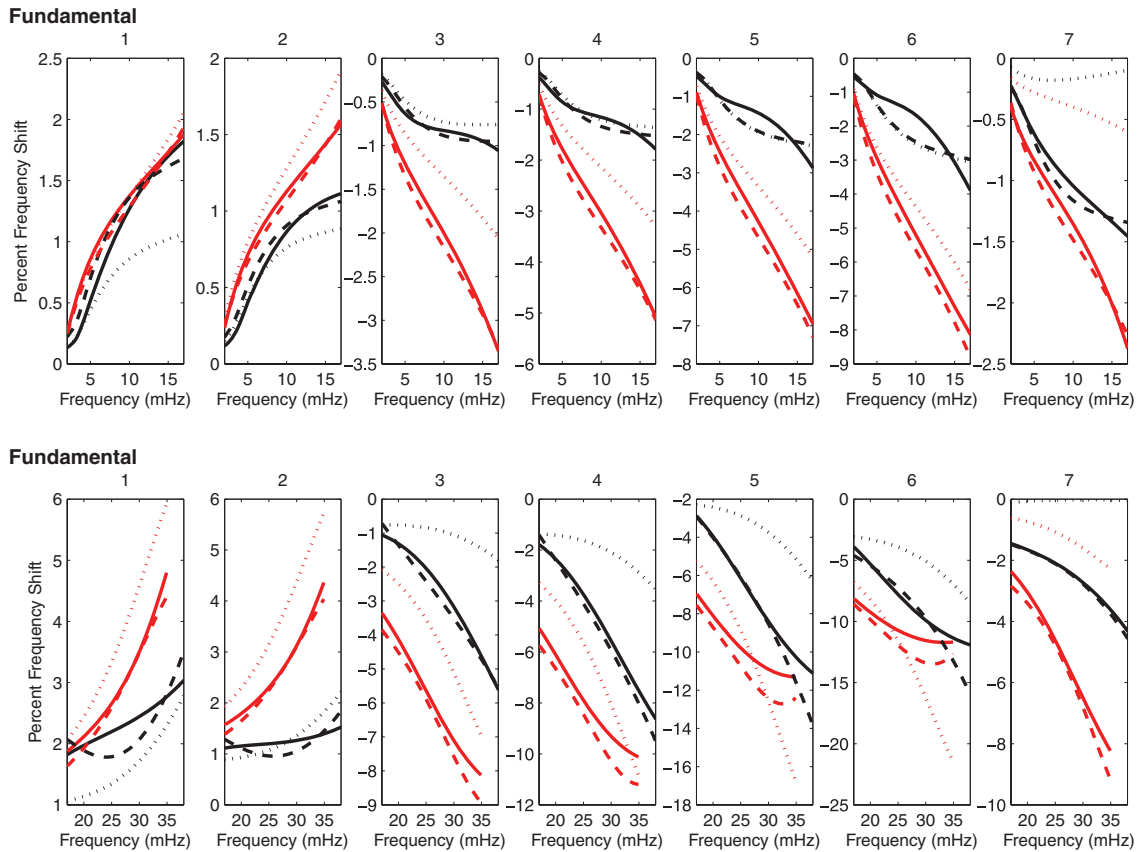


Figure 4. Frequency shifts of the fundamental toroidal (red) and spheroidal (black) due to differences in crustal structure between each of the canonical crustal types shown in Figs 1 and 3. Solid lines denote non-linear corrections ($\delta\omega_k^{NL}$), dotted lines indicate linear corrections ($\delta\omega_k^{SL}$), and the dashed lines indicate linear corrections improved using the method outlined in this paper ($\delta\omega_k^{ML}$). Only Moho corrections are applied in the upper row, while corrections for both surface and Moho topography are required by the broader frequency range of the bottom row.

5 METHOD VALIDATION

Having devised the MLC method for improving standard linear crustal corrections, we attempt to validate it by comparing its ability to predict crustal effects on waveforms against that of standard linear crustal corrections.

5.1 Application to a synthetic data set

The advent of fully numerical global wave propagation codes, such as the coupled Spectral Element Method (cSEM Capdeville *et al.* 2003), now allows accurate modelling of wave propagation through highly heterogeneous media such as the Earth's crust (e.g. Komatitsch & Tromp 2002). This advance offers us the opportunity to quantify how well standard approximate techniques for treating crustal effects perform when applied to tomographic inversions based on waveform modelling.

To this end, we generate a synthetic data set of long-period three-component waveforms for a set of 67 earthquakes selected from the global CMT catalogue. We ensure a realistic station distribution by only using stations at which the waveforms observed from the actual earthquake are sufficiently well recorded that they would be used in our global tomographic inversions. For a more detailed description of the data-selection criteria, see Mégnin & Romanowicz (2000). Fig. 6 shows the event and station distribution as well as ray path density of the synthetic data set.

Our velocity model has a spherically symmetric velocity profile which is identical to PREM (Dziewonski & Anderson 1981) below the 400 km discontinuity. At depths shallower than 400 km, the model is inverted to fit long-period waveforms starting from one of the physical reference models (Cammarano *et al.* 2005), which are calculated from a fixed composition (dry pyrolite) and a thermal profile using the elastic and anelastic properties of principal mantle minerals. The mantle model is radially anisotropic above 220 km, by the same amount as PREM. The crustal model has average crustal velocities and thicknesses from CRUST2.0 (Bassin & Masters 2000) filtered by a 5.6° Gaussian filter to avoid spatial aliasing by the SEM mesh. Topography from ETOPO1 (Amante & Eakins 2008) is similarly filtered. Effects of the ocean, ellipticity, gravity, rotation and anelasticity are all accounted for. The synthetic seismograms have energy at periods between 60 and 400 s, while earthquake source parameters are taken from the global CMT catalogue.

5.2 Mantle contamination due to crustal structure

We start by expressing the Moho topography of CRUST2.0 and topography of ETOPO1 using a spherical spline expansion characterized by 642 knots and an average interknot spacing of 7.9° (see Wang & Dahlen 1995). This is done for two reasons: (1) it imposes smoothness on the resulting model, as has to be done in actual global tomographic inversions; (2) it reduces the number of

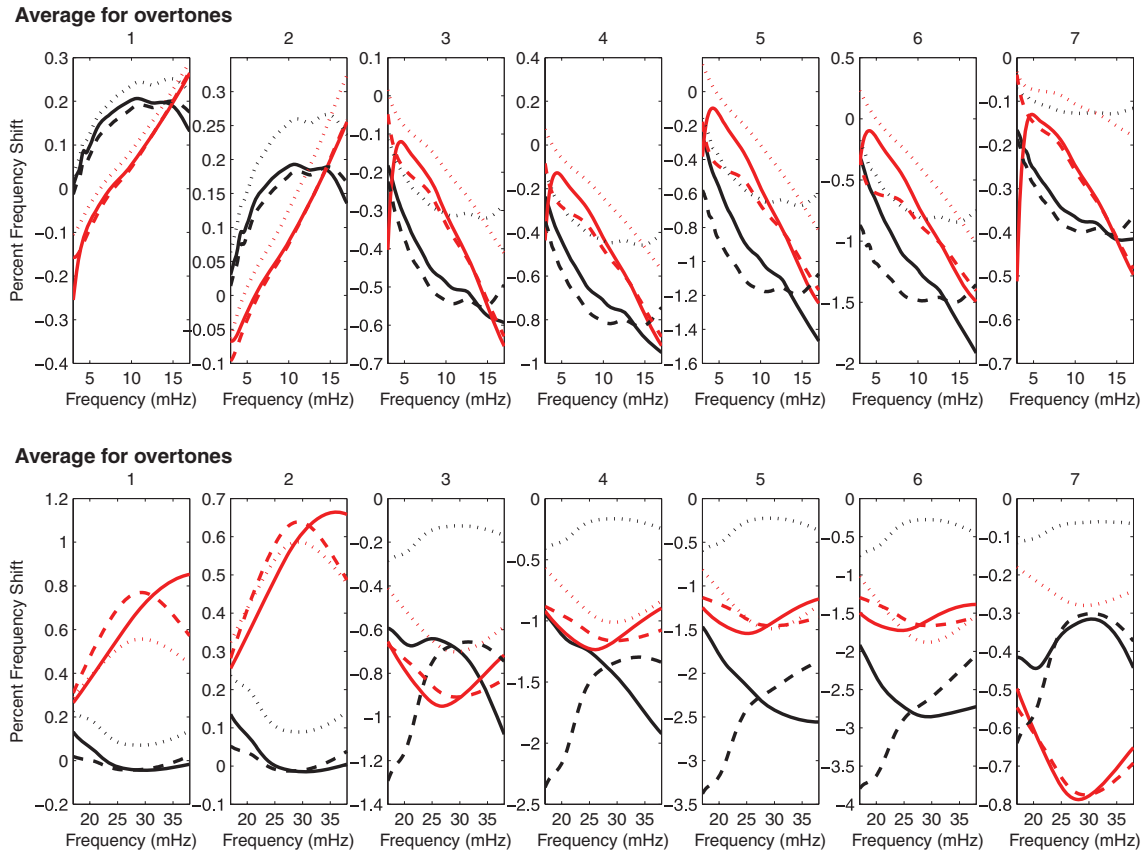


Figure 5. Average frequency shifts of the first five overtone toroidal (red) and spheroidal (black) branches due to differences in crustal structure between each of the canonical crustal types shown in Figs 1 and 3. Solid lines denote non-linear corrections ($\delta\omega_k^{NL}$), dotted lines indicate linear corrections ($\delta\omega_k^{SL}$), and the dashed lines indicate linear corrections improved using the method outlined in this paper ($\delta\omega_k^{ML}$). Only Moho corrections are applied in the upper row, while corrections for both surface and Moho topography are required by the broader frequency range of the bottom row.

coupling calculations that need to be considered in eq. (7). We then use both SLC and MLC approaches to predict the effects of the crust on the waveforms that make up our synthetic data set.

Fig. 7 shows a comparison of transverse-component accelerograms calculated using SEM and NACT with standard and modified linear corrections for the earthquake C032401C recorded at eight stations. When standard linear corrections are used, large phase-shifts are apparent for long continental paths, and are especially large on the transverse component, since Love waves are more sensitive to crustal structure than are Rayleigh waves. For Rayleigh waves, phase-shifts and amplitude discrepancies are apparent, but are much smaller, since linear corrections are more accurate (see Fig. 4). Waveforms predicted by our modified crustal corrections fit the SEM far better, and the improvement on continental paths is dramatic. Typically, the use of modified corrections for fundamental mode surface waves decreases the variance between SEM and NACT synthetics by ~ 65 per cent on the transverse and ~ 35 – 40 per cent on the radial and vertical components. When only overtone wavepackets are considered, modified linear crustal corrections reduce the variance by ~ 30 – 40 per cent for all the components.

The NACT synthetics are used to correct the SEM synthetic waveforms for the crustal effects. Two sets of residuals are produced, one resulting from applying standard linear corrections, and the other from our modified method. These residuals, which would ideally be very small, are then inverted for mantle structure. The data are weighted by a diagonal covariance matrix which serves to equalize lateral sensitivity, as proposed by Li & Romanowicz (1996). The

upper mantle is parametrized laterally with 642 spherical splines, and in depth by five cubic splines centred at depths of 24, 121, 221, 321 and 471 km (see Mégnin & Romanowicz 2000). At each point, we solve for two parameters—isotropic shear wave speed $V_S^2 = (2V_{SV}^2 + V_{SH}^2)/3$ and anisotropic parameter $\xi = V_{SH}^2/V_{SV}^2$ —and use scaling relations to obtain V_{PV} , V_{PH} and η , as in Panning & Romanowicz (2004). The inversion procedure is iterative and is stabilized by the introduction of an *a priori* model covariance matrix, as described in Tarantola & Valette (1982). Any retrieved mantle structure is interpreted as an artefact of unmodelled crustal structure, and will henceforth be referred to as contamination. Therefore, if the residuals efficiently map into mantle structure, then the inadequacies of crustal corrections can be expected to strongly contaminate existing mantle models. If, on the other hand, the residuals cannot be effectively modelled by mantle structure, then they are less likely to contaminate the mantle model.

Fig. 8 shows variations of isotropic shear wave speed obtained from the inversion of the residuals calculated using SLC as well as our MLC approach. Both fundamental mode and overtone wavepackets are used. The final model obtained with SLC explains a larger fraction of the starting variance in the residual seismograms than does the model obtained using modified corrections. This means that the inaccuracies of SLC can be more easily modelled by mantle structure than the inaccuracies of the MLC technique we propose; therefore, the use of SLC will contaminate mantle structure much more strongly than the use of MLC. For fundamental modes, the model obtained using SLC explains 64 per cent of

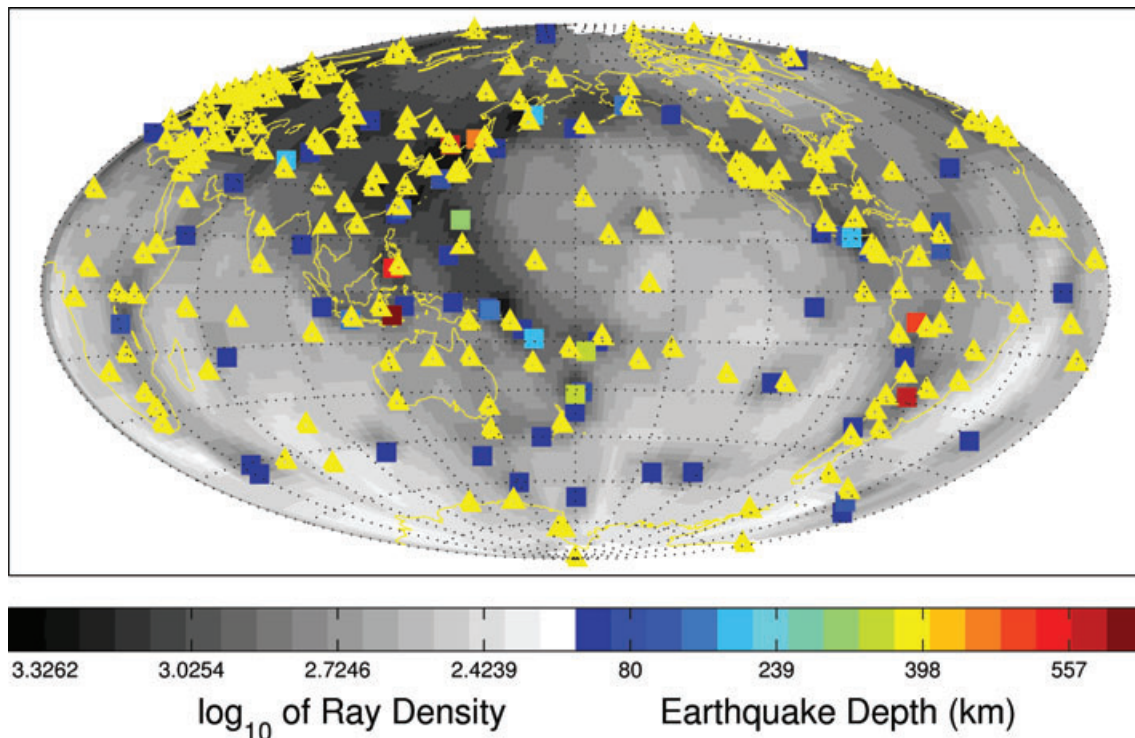


Figure 6. Map showing earthquake and station distribution of our synthetic data set. Earthquakes (squares) are colour-coded by depth, while the stations are denoted by yellow triangles. The shading is proportional to the log of the number of ray paths at that location.

the residuals on the longitudinal, 76 per cent on the transverse, and 80 per cent on the vertical component, whereas the model obtained using MLC reduced the starting misfit by 44 per cent for the longitudinal, 32 per cent for the transverse and 70 per cent for the vertical component. For overtones, the obtained model explains 47 per cent of the misfit on the longitudinal, 42 per cent on the transverse, and 57 per cent on the vertical component. Interestingly, the model obtained from MLC residuals only marginally improved the fit to the overtones (ranging from no improvement on the transverse component to 14 per cent on the vertical). This indicates that the correction factors succeeded in eliminating nearly all of the mantle contamination arising from the use of SLC.

Anisotropic structure was held fixed during the first two iterations, and was allowed to vary in the final 2 iterations. At each step of the inversion process, a range of *a priori* model parameter variances was explored; small values muted, while large values increased the amplitude of the retrieved structure. Misfits were calculated for all of the resulting models, and we chose a preferred *a priori* variance to be a compromise between achieving large variance reductions and keeping model size small. All parameters have a correlation length scale of 1000 km in the horizontal direction and 100 km in the vertical, which is similar to that imposed by the parametrization itself. Regardless of *a priori* variances, the retrieved pattern of mantle contamination remained the same.

Note the strong tectonic character of the mantle contamination, which is seismically slow beneath continents, where SLC underpredicts the effects of crustal structure. In particular, anomalously slow regions underlying mountain ranges (e.g. North American Cordillera) appear down to 100 km depth. At greater depths, most of the contamination is under the oceans, following the mid-ocean ridge systems, where the contamination is seismically fast. When MLC is used, we can see a significant reduction of contamination, especially at shallowest depths. Mantle beneath the North

American Cordillera, for instance, is nearly free of contamination even at 40 km depth. Contamination beneath the oceans is effectively suppressed. In fact, the tectonic character of the contamination becomes less prominent, and less well organized. It bears reminding that some of the remaining contamination might well result from the imperfect distribution of crossing paths afforded by our modest synthetic data set.

The sensitivity kernels shown in Fig. 2 show that the Love waves are significantly more sensitive to shallow layer structure than are Rayleigh waves. This fact, combined with other differences in the way that oceanic and continental crust affect Rayleigh and Love waves (see Bozdağ & Trampert 2008), suggests that inadequacies in crustal modelling can map efficiently into mantle anisotropic structure. Indeed, our maps of lateral variations in ξ confirm this suspicion. Fig. 9 shows the contamination of ξ that results from the use of standard and modified linear corrections. The maps shown are for the same model as in Fig. 8.

When SLC is applied, we retrieve enhanced V_{SV} to V_{SH} ratios, indicated by warm colours in Fig. 9, below both continents and oceans. Nevertheless, contamination is stronger beneath continents, and is particularly prominent beneath cratons. Beneath Tibet, as well as the Canadian and Brazilian cratons, this contamination extends to 225 km depth. Structure beneath the oceans also shows anomalously high ξ that tracks along the mid-ocean ridge system; this signature peters out around 150 km depth. MLC successfully suppresses contamination in all tectonic settings. In fact, signatures of all of the cratons except a small portion of the Brazilian craton are completely removed. Anomalous structure beneath Tibet becomes very weak as shallow as 100 km depth. Beneath oceans, no coherent contamination extends below 100 km depth.

Figs 8 and 9 attest to the ability of our modified linear corrections to minimize contamination of mantle isotropic and radially anisotropic structure that could result from the use of standard

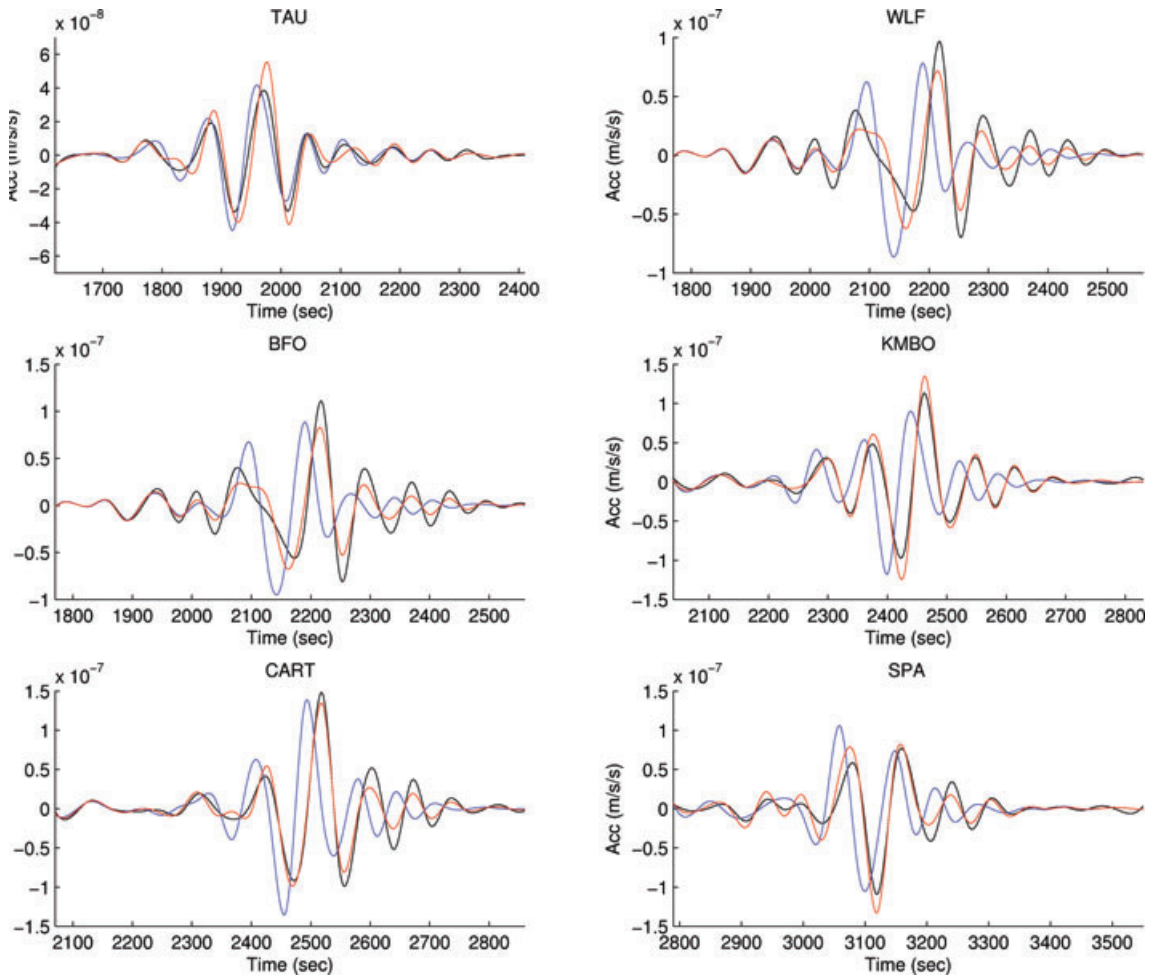


Figure 7. Comparison of Love waves predicted by SEM (black), standard linear corrections using NACT (blue), and our modified linear corrections using NACT (red). The earthquake is C032401C. The path to station TAU is largely oceanic, so both linear and modified corrections are capable of capturing the true crustal effect. This is not the case for continental paths, for which the use of standard linear corrections results in very large phase shifts. The modified crustal corrections do much better.

linear corrections. The success of our modifications is summarized in Fig. 10, which plots as a function of depth the contamination reduction (the percentage reduction in the size of the spurious model recovery) for both the V_s and ξ models resulting from the use of modified instead of standard linear corrections. We define the contamination reduction at radius r as

$$CR(r) = \int_{\theta} \int_{\phi} \frac{m_{slc}^2(r, \theta, \phi) - m_{mlc}^2(r, \theta, \phi)}{m_{slc}^2(r, \theta, \phi)} d\theta d\phi, \quad (12)$$

where $m(r, \theta, \phi)$ denotes the value of the model at location (r, θ, ϕ) . At depths greater than 150 km, our modifications reduce the contamination of ξ mantle structure by more than half, and reduce by more than a third the contamination of isotropic structure at all depths.

5.3 Application to long period waveform data

Having demonstrated the potential of the proposed technique for reducing the contamination of mantle structure from unmodelled crustal effects, we proceed to apply the method to an actual waveform data set used in the creation of the SAW642AN model of Panning & Romanowicz (2006, henceforth PR06). The data set

consists of three-component long period surface ($T > 60$ s) and body wave ($T > 30$ s) packets from 1191 events, and is detailed in table 1 of PR06.

We employ identical data weighting and parametrization as that used in construction of SAW642AN. The primary difference is the removal of crustal effects via our modified linear corrections as opposed to the approximate, regionalized non-linear corrections used in PR06. We derive the final model after four iterations starting from SAW642AN. While we do not derive a specific set of modified linear corrections for body waves (and indeed, it is not obvious whether this approach, which does not take coupling between modes into account, would be appropriate for body wave data), we choose to correct the body wave data with the corrections derived for overtones, as it produces a better fit to the data than standard linear corrections. Regularization is chosen such that the final model size (as measured by the root-mean-squared amplitude of structure as a function of depth) closely matches that of SAW642AN for the isotropic portion of the model, and is matched or reduced in the anisotropic portion of the model.

The following two findings summarize the effects of the use of our modified linear crustal corrections on the retrieved mantle model: (1) The overall misfit to the data is reduced for all wavepacket

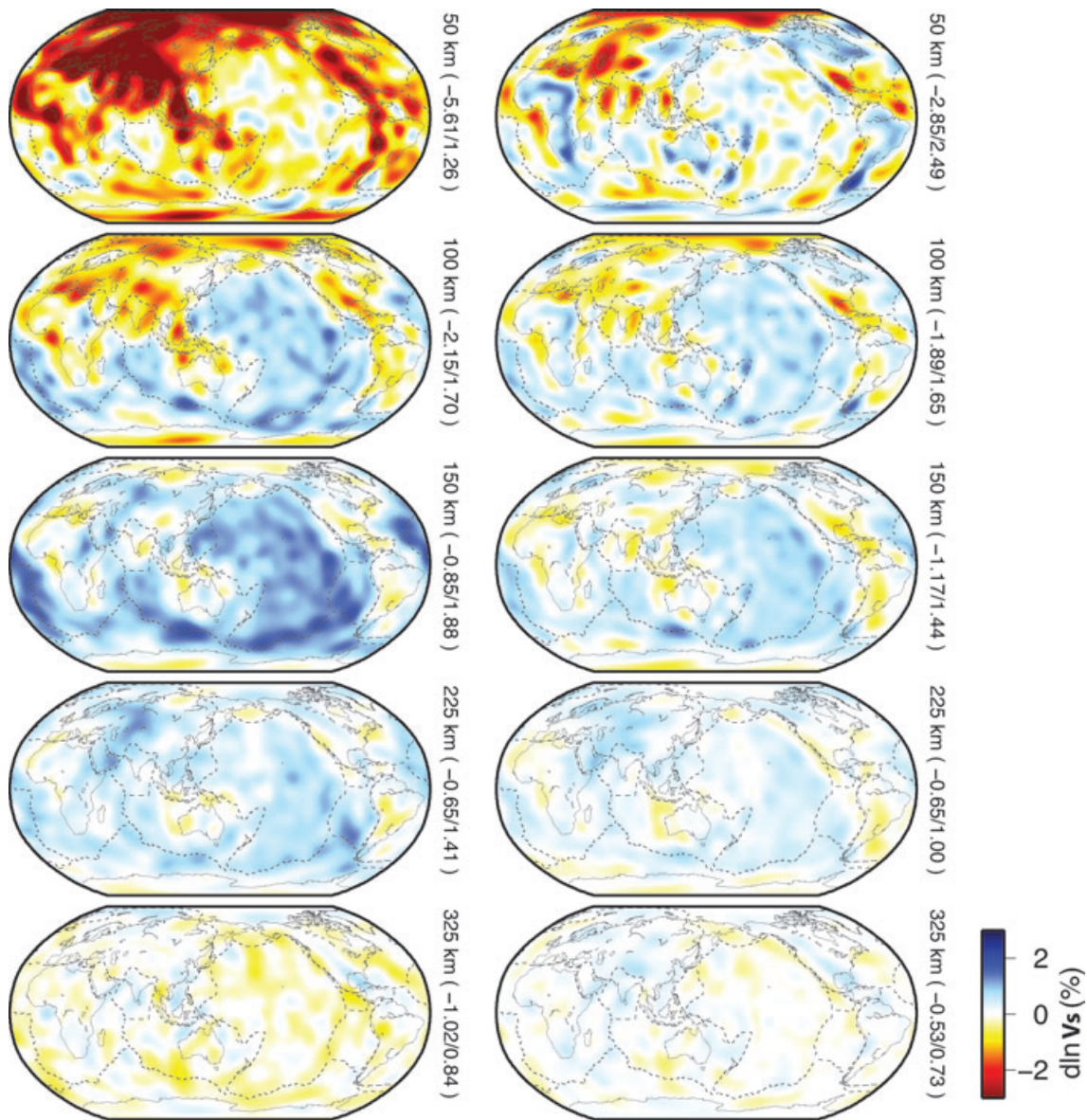


Figure 8. Expected contamination of mantle isotropic S -wave speed due to the use of standard (left-hand column) and our modified (right-hand column) linear crustal corrections on fundamental mode and overtone wavepackets. Warm (cool) colours indicate that using linear crustal corrections would artificially decrease (increase) retrieved mantle V_s . Note the significant amplitudes of contamination associated with standard linear corrections even at 150 km.

types (fundamental modes, overtones, and body waves); and (2) the anticorrelation of upper and mid-mantle isotropic V_s structure present in SAW642AN is diminished (see Fig. 11), bringing the model to closer agreement with other models of mantle shear wave speed (e.g. Kustowski *et al.* 2008). While the improvement in fit is not extremely large (variance reduction of the final model with the modified linear corrections is 54.5 per cent across all data types versus 52.1 per cent for SAW642AN using the regionalized non-linear corrections), it is important to note that the better fit is obtained with a model that is smaller in size, particularly in anisotropic structure, than the starting model. The detailed effects on the retrieved isotropic and anisotropic structure are more complicated and are discussed in a companion paper (Panning *et al.* 2010), which also explores the effects of damping and quantifies model uncertainties.

6 CONCLUSION AND DISCUSSION

We propose and validate a new method (modified linear corrections: MLC) for performing crustal corrections. The method is built around additive correction factors, which modify the topographies of crustal discontinuities; these modified topographies can then be used alongside SLC to mimic the non-linear effects of the true discontinuity topographies. The correction factors depend on the local crustal type, on the discontinuity considered, on the reference model used for calculating the sensitivity kernels, as well as mode type (spheroidal versus toroidal and fundamental versus overtone). The MLC method, while theoretically less accurate than the two-step NLC corrections that have been recently applied to global tomography, has far smaller computational costs, and can thus be applied to higher frequencies. In fact, once the correction factors have been

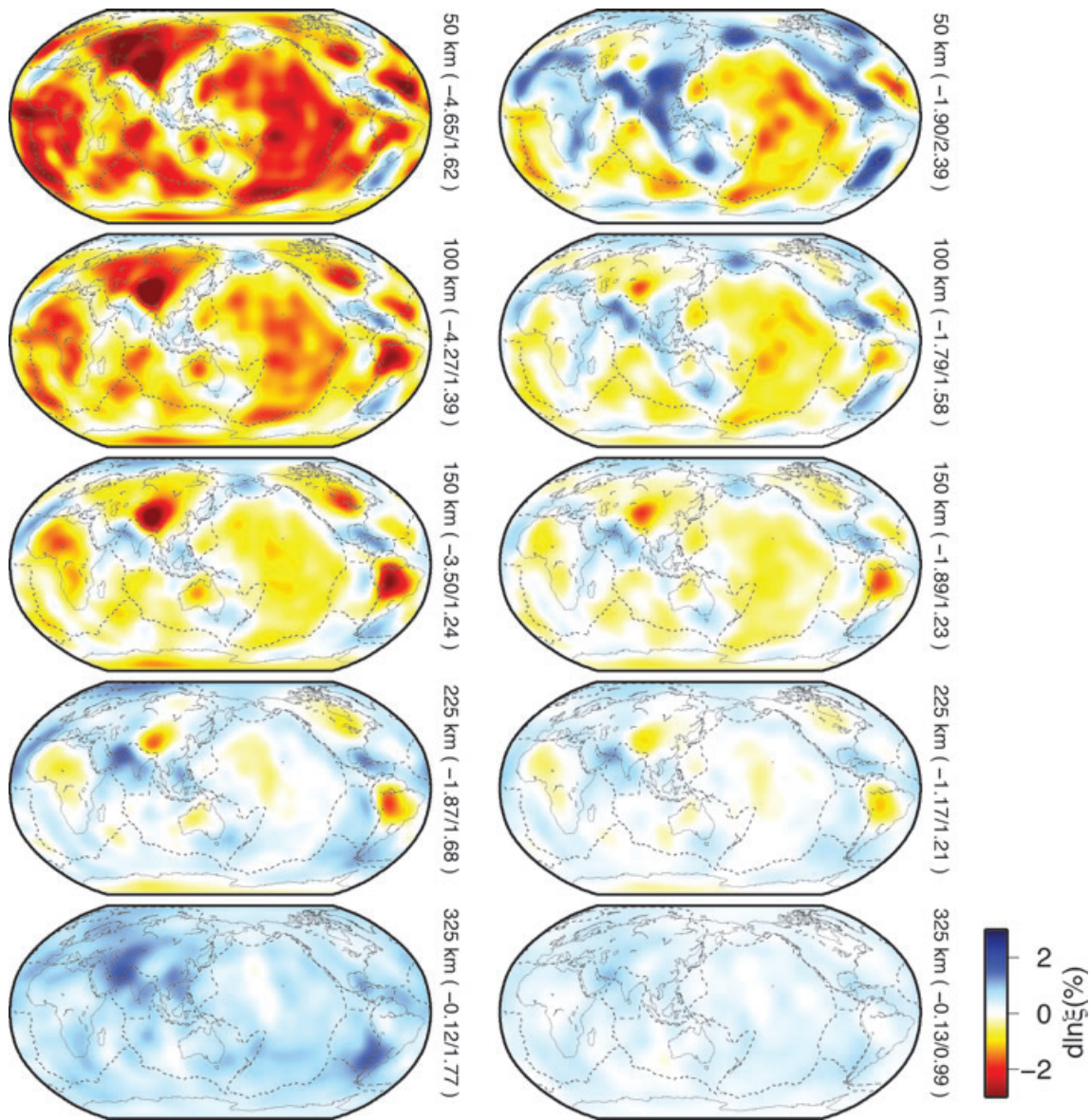


Figure 9. Expected contamination of mantle radial anisotropy due to the use of standard (left-hand column) and our modified (right-hand column) linear crustal corrections on fundamental mode and overtone wavepackets. Warm (cool) colours indicate that linear crustal corrections can cause artificially low (high) ξ ($V_{SV} > V_{SH}$ versus $V_{SH} > V_{SV}$). Note the large amplitudes of spurious anisotropic structure resulting from the use of standard linear corrections. Modified linear corrections result in significant reduction in contamination of anisotropic structure at all depths.

calculated, MLC requires no additional computations beyond those of SLC. Its computational efficiency allows for a greater number of reference velocity profiles to be used than is typical in the NLC approach.

We validate the MLC approach against a synthetic data set, and quantify its performance against that of SLC. The synthetic data set is calculated at long periods (>60 s) for a 3-D crustal model and a 1-D mantle using the Spectral Element Method. The synthetic waveforms are corrected for the effects of the known crustal structure using both MLC and SLC approaches, and the resulting residuals are inverted for a mantle model. Thus, we obtain images of upper mantle contamination that may result from inadequate crustal corrections. These tests show that the substantial contamination of isotropic mantle structure down to depths of 150 km resulting from the use of SLC is reduced by >30 per cent by MLC. Specifically, at depths shallower than 100 km, SLC will artificially reduce mantle

V_s beneath continents; at greater depths, SLC will make oceanic ridges appear artificially fast. Due to differences in crustal sensitivity of Rayleigh and Love waves, the deleterious effects of SLC on anisotropic structure are far more severe, and can potentially obliterate the mantle anisotropic signal in the upper 200 km. When the MLC approach is used, much of the mantle contamination is removed; indeed, the contamination of anisotropic parameter ξ is reduced by more than half at depths below 125 km. Thus, MLC's separate treatment of toroidal and spheroidal modes and fundamental modes and overtones proved to be highly successful in suppressing the contamination of radial anisotropy in the mantle.

Our tests with the synthetic SEM data set shows that the MLC method improves the accuracy of linear corrections equally well for fundamental modes as for overtones, though the total crustal signal is, unsurprisingly, far larger for the fundamental mode surface waves. Since the additive correction factors were calculated only

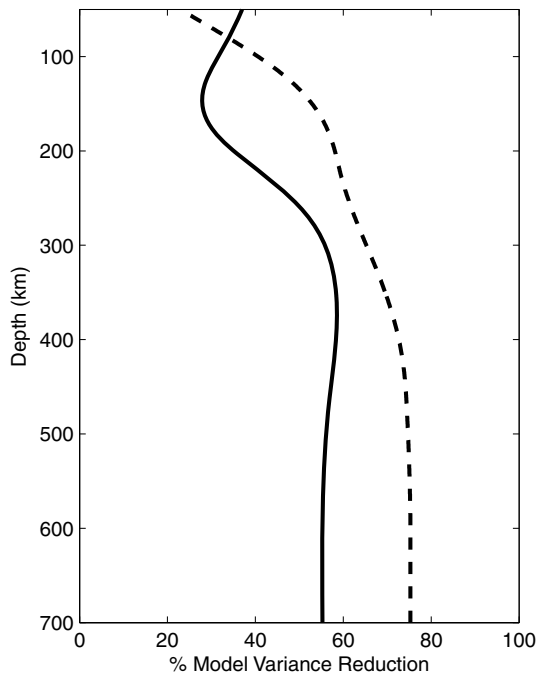


Figure 10. Relative variance reduction in percent resulting from the use of modified linear corrections for the V_s (solid line) and ξ (dashed line) structure as a function of depth.

accounting for coupling within multiplets, their success at modelling the true effects of crustal structure on overtones indicates that the non-linear crustal effects on multiplet–multiplet coupling are similar to those on coupling within a multiplet. This justifies our choice to neglect multiplet–multiplet coupling when calculating the additive correction factors.

In addition to the synthetic tests, we apply our new method for improving crustal corrections to the waveform data set used to construct SAW642AN (Panning & Romanowicz 2006). We find that the better treatment of crustal structure improves the fit to the data for all wavepacket types (body waves, surface waves and overtones alike). Furthermore, it eliminates anticorrelation between upper and mid mantle structure which distinguished SAW642AN from other global models of mantle shear wave speed structure.

Though the primary focus of our paper was the development of a computationally inexpensive technique to account for the non-linear effects of the crust on surface wave and overtone waveforms, the SEM-based validation data set also allowed us, for the first time in global waveform tomography, to quantify the contamination of mantle structure that may arise from the use of inadequately accurate crustal corrections. We have shown that crustal corrections can contaminate isotropic, but especially anisotropic structure, to great depths. Our results confirm earlier findings of Bozdağ & Trampert (2008), who also investigated the accuracy of fully non-linear approaches akin to NLC, but did not analyse full waveforms or overtones. Our results have great bearing on recent efforts at validating existing tomographic models developed with approximate wave propagation techniques using more accurate numerical approaches, such as SEM (e.g. Qin *et al.* 2009). This is because tomographic models of mantle structure were developed by predicting and correcting for the effects of crustal structure, and are likely to correctly predict seismic waveforms only when used alongside their associated crustal corrections. Our work implies that implementing these crustal models in SEM is likely to result in very

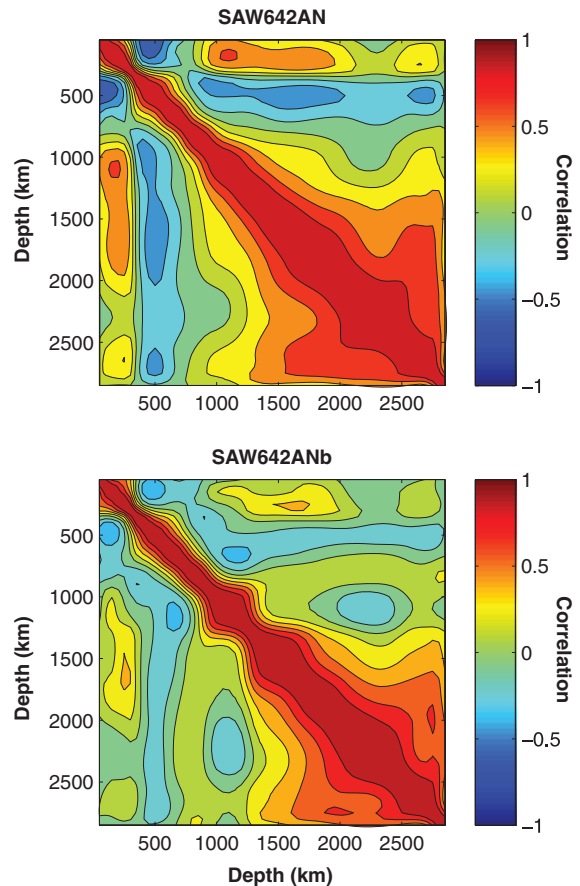


Figure 11. Radial correlation functions for the SAW642AN model (top) and a model derived from identical data but in which the crustal corrections were performed using modified linear corrections proposed here (bottom). Note that the use of modified linear corrections nearly eliminates the anticorrelation between upper and mid mantle structure apparent in SAW642AN. This anticorrelation is not seen in most other global models of shear wave speed.

different crustal effects than those used to develop the mantle model. Since the effects of the crust are much larger for horizontally polarized shear waves, a straightforward crustal implementation in SEM is likely to find that models developed using horizontally polarized shear waves are less able to explain the observed waveforms than V_s models. Indeed, this is consistent with the findings of Qin *et al.*

The remaining inadequacies of our modified crustal corrections are likely due to off-path effects, source effects, limitations imposed by parametrization, as well as the approximate nature of our method. Our approach can easily be combined with methods that take into account lateral sensitivity of surface waves. Accuracy of the method can be improved by considering a larger set of crustal types that would better capture the true variability in Earth's crustal structure, as well as topographies of intracrustal discontinuities (such as the Conrad). We note that while increasing the number of crustal types and discontinuities would make the calculation of the correction factors more computationally costly, it would not increase computational costs associated with using the modified discontinuity topographies. The modified linear crustal corrections that we have outlined in this paper also present an advantage over numerical techniques such as the finite element or spectral element codes since they are capable of, albeit approximately, accounting for the effects

of near-surface, thin sedimentary layers; incorporating sedimentary basins in finite or spectral element codes vastly increases their already large computational costs. Thus, we believe that the method presented here is particularly well-suited for taking advantage of ever-improving knowledge of crustal structure.

ACKNOWLEDGMENTS

The authors would like to thank Yann Capdeville for providing us the cSEM code. Support for VL was provided in part by a National Science Foundation Graduate Fellowship. We acknowledge support from NSF (grant EAR-0738284). This is Berkeley Seismological Laboratory contribution 10-06.

REFERENCES

- Amante, C. & Eakins, B.W., 2008. ETOPO1 1 Arc-Minute Global Relief Model: Procedures, Data Sources and Analysis, National Geophysical Data Center, NESDIS, NOAA, U.S. Department of Commerce, Boulder, CO.
- Bassin, C.G.L. & Masters, G., 2000. The current limits of resolution for surface wave tomography in North America, *EOS, Trans. Am. geophys. Un.*, **81**, Fall Meeting Supp., abstract S12A-03.
- Boschi, L. & Ekström, G., 2002. New images of the Earth's upper mantle from measurements of surface wave phase velocity anomalies, *J. geophys. Res.*, **107**, doi:10.1029/2000JB000059.
- Bozdag, E. & Trampert, J., 2008. On crustal corrections in surface wave tomography, *Geophys. J. Int.*, **172**, 1066–1082.
- Cammarano, F., Deuss, A., Goes, S. & Giardini, D., 2005. One-dimensional physical reference models for the upper mantle and transition zone: combining seismic and mineral physics constraints, *J. geophys. Res.*, **110**, B01306, doi:10.1029/2004JB003272.
- Capdeville, Y., Chaljub, E., Vilotte, J.P. & Montagner, J.P., 2003. Coupling the spectral element method with a modal solution for elastic wave propagation in global earth models, *Geophys. J. Int.*, **152**, 34–67.
- Chevrot, S. & Zhao, L., 2007. Multiscale finite-frequency Rayleigh wave tomography of the Kaapvaal craton, *Geophys. J. Int.*, **169**, 201–215.
- Dahlen, F. & Tromp, J., 1998. *Theoretical Global Seismology*, University Press, Princeton.
- Dziewonski, A.M. & Anderson, D.L., 1981. Preliminary reference Earth model, *Phys. Earth planet. Inter.*, **25**, 297–356.
- Gu, Y.J., Dziewonski, A.M. & Ekström, G., 2003. Simultaneous inversion for mantle shear velocity and topography of transition zone discontinuities, *Geophys. J. Int.*, **154**, 559–583.
- Komatitsch, D. & Tromp, J., 2002. Spectral-element simulations of global seismic wave propagation-II. Three-dimensional models, oceans, rotation and self-gravitation, *Geophys. J. Int.*, **150**, 303–318.
- Kustowski, B., Dziewonski, A. & Ekstrom, G., 2007. Nonlinear crustal corrections for normal-mode seismograms, *Bull. seism. Soc. Am.*, **97**(5), 1756–1762.
- Kustowski, B., Ekström, G. & Dziewonski, A.M., 2008. Anisotropic shear-wave velocity structure of the Earth's mantle: a global model, *J. geophys. Res.*, **113**, B06306, doi:10.1029/2007JB005169.
- Li, X.-D. & Romanowicz, B., 1995. Comparison of global waveform inversions with and without considering cross-branch modal coupling, *Geophys. J. Int.*, **121**, 695–709.
- Li, X.-D. & Romanowicz, B., 1996. Global mantle shear velocity model developed using nonlinear asymptotic coupling theory, *J. geophys. Res.*, **101**, 22 245–22 272.
- Li, X. & Tanimoto, T., 1993. Waveforms of long-period body waves in a slightly aspherical Earth model., *Geophys. J. Int.*, **112**, 92–102.
- Marone, F. & Romanowicz, B., 2007. Non-linear crustal corrections in high-resolution regional waveform seismic tomography, *Geophys. J. Int.*, **170**, 460–467.
- Mégnin, C. & Romanowicz, B., 2000. The three-dimensional shear velocity structure of the mantle from the inversion of body, surface and higher-mode waveforms, *Geophys. J. Int.*, **143**, 709–728.
- Meier, U., Curtis, A. & Trampert, J., 2007. Fully nonlinear inversion of fundamental mode surface waves for a global crustal model, *Geophys. Res. Lett.*, **34**, L16304, doi:10.1029/2007GL030989.
- Montagner, J.-P. & Jobert, N., 1988. Vectorial tomography II. Application to the Indian Ocean, *Geophys. J.*, **94**, 309–344.
- Montagner, J.-P. & Tanimoto, T., 1991. Global upper mantle tomography of seismic velocities and anisotropies, *J. geophys. Res.*, **96**, 20 337–20 351.
- Mooney, W.D., Laske, G. & Guy Masters, T., 1998. CRUST 5.1: a global crustal model at 5 deg × deg, *J. geophys. Res.*, **103**, 727–748.
- Nataf, H. & Ricard, Y., 1996. 3SMAC: an a priori tomographic model of the upper mantle based on geophysical modeling, *Phys. Earth planet. Inter.*, **95**, 101–122.
- Panning, M. & Romanowicz, B., 2004. Inference on Flow at the Base of the Earth's Mantle Based on Seismic Anisotropy, *Science*, **303**, 351–353.
- Panning, M. & Romanowicz, B., 2006. A three-dimensional radially anisotropic model of shear velocity in the whole mantle, *Geophys. J. Int.*, **167**, 361–379.
- Panning, M., Lekic, V. & Romanowicz, B., 2010. The importance of crustal corrections in the development of a new global model of radial anisotropy, *J. geophys. Res.*, submitted.
- Pasyanos, M.E., 2005. A variable resolution surface wave dispersion study of Eurasia, North Africa, and surrounding regions, *J. geophys. Res.*, **110**(B9), B12301, doi:10.1029/2005JB003749.
- Qin, Y., Capdeville, Y., Montagner, J., Boschi, L. & Becker, T., 2009. Reliability of mantle tomography models assessed by spectral element simulation, *Geophys. J. Int.*, **177**(1), 125–144.
- Ritsema, J., van Heijst, H.J. & Woodhouse, J.H., 2004. Global transition zone tomography, *J. geophys. Res.*, **109**, B02302, doi:10.1029/2003JB002610.
- Romanowicz, B., 1987. Multiplet-Multiplet coupling due to lateral heterogeneity: asymptotic effects on the amplitude and frequency of the Earth's normal modes, *Geophys. J. Int.*, **90**, 75–100.
- Romanowicz, B., Panning, M., Gung, Y. & Capdeville, Y., 2008. On the computation of long period seismograms in a 3D earth using normal mode based approximations, *Geophys. J. Int.*, **175**(2), 520–536.
- Stutzmann, E. & Montagner, J.-P., 1994. Tomography of the transition zone from the inversion of higher-mode surface waves, *Phys. Earth planet. Inter.*, **86**, 99–115.
- Tarantola, A. & Valette, B., 1982. Generalized nonlinear inverse problems solved using the least squares criterion, *Rev. Geophys. Space Phys.*, **20**, 219–232.
- Wang, Z. & Dahlen, F.A., 1995. Spherical-spline parametrization of three-dimensional Earth models, *Geophys. Res. Lett.*, **22**, 3099–3102.
- Woodhouse, J.H., 1998. The calculation of eigenfrequencies and eigenfunctions of the free oscillations of the Earth and the Sun, in *Seismological Algorithms*, pp. 321–370, ed. Doornbos, D.J., Elsevier, New York.
- Woodhouse, J.H. & Dahlen, F.A., 1978. The effect of a general aspherical perturbation on the free oscillations of the earth, *Geophys. J. R. astr. Soc.*, **53**, 335–354.
- Woodhouse, J.H. & Dziewonski, A.M., 1984. Mapping the upper mantle: three dimensional modeling of earth structure by inversion of seismic waveforms, *J. geophys. Res.*, **89**, 5953–5986.
- Woodhouse, J.H. & Girnius, T.P., 1982. Surface waves and free oscillations in a regionalized earth model, *Geophys. J. R. astr. Soc.*, **68**, 653–673.